diffusion-fundamentals.org

The Open-Access Journal for the Basic Principles of Diffusion Theory, Experiment and Application

Crossover from Single-File to Fickian Diffusion in Carbon Nanotubes and Nanotube Bundles: Pure Components and Mixtures

Ying-Chun Liu[2,1*], *Joshua D. Moore*[1*] , *Qu Chen*[2], *Thomas J. Roussel*[1,†], *Qi Wang*[2], *and Keith E. Gubbins*[1]

1. Department of Chemical and Biomolecular Engineering, North Carolina State University, Raleigh, NC, 27695-7905, USA
2. Department of Chemistry, Zhejiang University, Hangzhou, 310027, P.R. China

Corresponding author:
Ying-Chun Liu
Department of Chemistry, Zhejiang University
Hangzhou, 310027, P.R. China
E-Mail: liuyingch@zju.edu.cn

Abstract

The diffusion mechanism of pure component Ar and binary mixtures of Ar/Kr and Ar/Ne confined in single-walled carbon nanotubes (SWNTs) and bundles was investigated by a combined Grand Canonical Monte Carlo and molecular dynamics study. For Ar confined in SWNTs, a crossover from single-file to Fickian diffusion existed when the density of Ar was a minimum as a function of the SWNT diameter. Argon diffused by a single-file mechanism in SWNTs smaller than an accessible diameter of $1.76\sigma_{Ar}$, corresponding to (7,7), (12,0) and (8,6) SWNTs but by a Fickian mechanism for SWNTs larger in diameter. Both components in Ar/Kr mixtures had a single-file diffusional mechanism in (6,6) and (7,7) SWNTs and a Fickain mechanism for SWNTs larger in diameter. Likewise, both components in a Ar/Ne mixtures had a single-file diffusional mechanism in a (6,6) CNT, and Ar had a single-file diffusional mechanism in a (7,7) SWCNT. However, Ne in the Ar/Ne mixture exhibited Fickian diffusion in the (7,7) SWNT , which indicated bi-modal diffusion. Larger diameters of SWNTs provided Fickian diffusion for both components in an Ar/Ne mixture. Argon diffused in a (25,0) SWNT bundle (with a bimodal pore size distribution) in a bimodal mechanism, with Ar diffusing in single-file in interstitial sites and in a Fickian mechanism in inner nanotube channels. In all cases of single-file diffusion the mean-squared displacement (MSD) of the fluid molecules had a square root of time dependence, while molecules diffusing by a Fickian mechanism had a MSD with a linear time dependence.

Keywords: single-file; Fickian; carbon nanotubes; bundle; diffusion mechanism; bimodal diffusion

---

[*] These authors contributed equally to this work.

[†] Current Address: Institut de Ciència de Materials , Consejo Superior de Investigaciones Científicas, Campus de la UAB, 08193, Bellaterra, Barcelona, Spain

1. Introduction

The unique properties of single-walled carbon nanotubes (SWNTs) and their potential applications make them important materials [1,2] in the fields of material science, physics, chemistry, and biology [3, 4, 5, 6, 7, 8, 9]. It is therefore of practical interest to understand the properties that govern the diffusion mechanism of molecules confined in carbon nanotube structures [10, 11, 12]. Three types of mechanism of self-diffusion are known to occur in small pores. Ballistic motion occurs for very short times, before molecules have had a chance to collide, and the mean squared displacement of the molecules is proportional to time squared. For longer times the motion becomes either Fickian or single-file. If the pore is large enough, the molecules will diffuse in 3 dimensions as they would in a bulk fluid, and the mean squared displacement is proportional to time. In confinement, as the diameter of the pore becomes smaller, the diffusion will crossover from 3 dimensions to single-file diffusion, where the molecules can no longer pass each other. The mean square displacement for single-file diffusion is proportional to the square root of time.

Single-file diffusion (SFD) can be important for our understanding of catalysis in one-dimensional pores or for the use of hydrocarbon traps for automobile applications [13]. In these applications the effective control of transport requires a deep understanding of the governing diffusion mechanisms. However, the mechanisms by which molecules flow through nanoporous materials are currently not well understood and are difficult to determine experimentally, especially for materials having hierarchical pore structures.

Single-file diffusion has been observed experimentally for small molecules in zeolites [14, 15, 16] and for colloid particles in one-dimensional channels [17]. It has been demonstrated for hard spheres in spherical tubes with hard walls in simulations [18, 19, 20] and is also predicted theoretically [21, 22]. Percus and Levitt's early work showed that SFD has a mean square displacement proportional to the square root of time [23,24]. Mon and Percus, using a model of hard sphere fluids in cylindrical pores with hard walls, presented a transition state theory of the transition from SFD to Fickian diffusion, in terms of a hopping time, defined as the average time a particle must spend before it can hop over its nearest neighbor [18]. They also numerically solved the multidimensional diffusion equation describing the time evolution of two hard disks diffusing in narrow hard channels [25] and the average time needed for a hard disk to hop past a nearest neighbor in the longitudinal direction [26].

There is a dramatic difference (several orders of magnitude) between the self-diffusion rates of a fluid in Fickian and single-file diffusion. It is therefore useful to be able to predict when these diffusion mechanisms will occur and the influence that variables such as pore diameter, host flexibility, adsorbate properties, and temperature have on the mechanism. Even though single-file diffusion has been predicted theoretically for decades, it is still far from well understood. In particular, most investigations involve hard sphere fluids in a model cylindrical pore with hard walls. It is therefore necessary to understand conditions between different diffusion mechanisms in realistic models of microporous materials with atomically detailed walls and continuous potentials. Here we give an overview of our work modeling confined fluids diffusing in SWNTs and SWNT bundles. We have investigated argon confined in SWNTs and in a

SWNT bundle, and binary Lennard Jones mixtures of argon/krypton and argon/neon in SWNTs. The goal of these studies focus on the crossover from single-file diffusion to Fickian diffusion, investigating the effects of the SWNT diameter and the density of the diffusing fluid.

2. Model and Simulation Details

In all of our simulations, the interactions between the adsorbate molecules as well as between the SWNT and the adsorbate molecules were described through a standard (12,6) Lennard-Jones potential. The SWNTs are rigid with the carbon atoms held fixed and are given zero velocity in the MD simulations. Parameters for argon and carbon were taken from Skoulidas and Sholl [27] (σ_{Ar} = 0.342 nm, ε_{Ar} / k_b = 124.07 K) and from Steele [28] (σ_C = 0.34 nm, ε_C / k_b = 28.0 K), respectively. All cross interactions were obtained through the usual Lorentz-Berthelot combination rules.

2.1 Pure Component argon in SWNTs

Grand Canonical Monte Carlo simulations (GCMC) were performed to compute argon adsorption isotherms in SWNTs at 298K . The fluid was restricted to adsorbing in the inner channels of the SWNTs only. Several chiralities (armchair, zigzag and chiral) of SWNTs, based on the two indices (n,m) of the Hamada classification [29], were studied. The armchair (*m,m*) SWNTs had indices of *n* = 6, 7, 8, 9, 10, corresponding to diameters of 0.81, 0.95, 1.08, 1.22, and 1.35 nm, respectively. The zigzag (*n*, 0) SWNTs had indices of *n* = 10, 11, 12, 13, 14, 15, corresponding to diameters of 0.78, 0.86, 0.94, 1.02, 1.09, 1.17 nm, respectively. The chiral (*m, n*) SWNTs had chiral indices of *m* =7, 8, 9, 10, 11 and *n* = 5, 6, 7, 8, 9, corresponding to diameters of 0.82, 0.95, 1.09, 1.22, and 1.36 nm, respectively. In the GCMC simulations, the nanotube lengths were 9.83 nm, 11.08 nm, and 8.90 to 14.76 nm in length for the armchair (*m,m*), zigzag (*n,0*), and chiral (*n,m*) geometries, respectively. The isotherm was measured in the range 8×10^{-5} to 30 MPa, the latter being a pressure at which all of the tubes were completely filled with adsorbate.

The molecular dynamics (MD) simulations for this set of simulations were performed using the NAMD (NAnoscale Molecular Dynamics) simulation package [30] using a Langevin thermostat with a damping coefficient of 1 ps^{-1}. The configurations from the GCMC simulations were used as a starting configuration for the MD simulations, but were replicated five times in the axial (*z*) direction of the nanotube. This corresponded to a range of 114 and 840 fluid atoms in the simulations. The MD simulations were performed using an equilibration period of at least 2 ns followed by a production run of at least 10 ns using a 1 fs timestep. The mean-squared displacement was measured in the axial direction of the nanotube from the trajectory of the production run. Periodic boundary conditions were used in the axial direction of the nanotube.

2.2 Binary mixtures of argon/krypton and argon/neon

We have chosen systems of armchair nanotubes solvated with binary mixtures of Lennard-Jones (LJ) fluids (argon(Ar)/krypton(Kr) and argon(Ar)/neon(Ne)). We varied

the mole fraction of each mixture in each tube from x_{Ar} = 0 to 1, while modifying the density of each component in the tube according to the following equation:

$$\rho_{mix} = x_{Ar}\rho_{Ar} + x_B\rho_B \tag{1}$$

In Eq. (1), ρ_{mix} is the mixture density, x_{Ar} is the mole fraction of argon, ρ_{Ar} is the pure component density of argon, x_B is the mole fraction of the second component in the mixture (i.e., Kr or Ne), and ρ_B is the pure component density of the second component in the mixture. By writing Eq. (1) we make an assumption that there is no volume change upon mixing of the two fluids. While this is not necessarily true, especially considering the confinement and high pressure of the mixtures confined inside the nanotubes, for the purpose of this study Eq. (1) is adequate as we are only interested in obtaining a range of densities and concentrations.

For this study we have selected the pure component densities at the state point of 298 K and 300 bar [31] based on the observation that for pure argon all of the nanotubes were completely filled at this pressure. The number of molecules of each component can be solved by equating Eq. (1) with Eq. (2).

$$\rho_{mix} = \frac{1}{N_{Av}}\left(\frac{n_A m_A}{V_A^{acc}} + \frac{n_B m_B}{V_B^{acc}}\right) \tag{2}$$

$$V_i^{acc} = \frac{\pi}{4}L\left[d_t - \left(\frac{\sigma_C + \sigma_i}{2}\right)\right]^2 \tag{3}$$

In Eq. (2) N_{Av} is Avogadro's number, n_i is the number of molecules of A or B, m_i is the molar mass of A or B, and V_i^{acc} is the accessible volume of A or B in the nanotube, as given by Eq. (3). The accessible volume is an estimate based upon the diameter of the nanotube (d_t), the length of the nanotube (L), and an estimate of the contribution due to the cross interaction between the fluid particles and carbon atoms at the wall. The estimate in Eq. (3) is based on the Lorrentz combining rule for the cross interaction, σ_{ij}.

$$\sigma_{ij} = \frac{\sigma_i + \sigma_j}{2} \tag{4}$$

The densities of the mixtures used are shown in Table 1 for mixtures of Ar/Kr and Ar/Ne. Additional LJ parameters were used for Kr [32] (σ_{Kr} = 0.3607 nm, ε_{Ar}/k_b = 161 K) and for Ne [27] (σ_{Ne} = 0.2789 nm, ε_{Ne}/k_b = 35.7 K). Note that in our study in 2.1, we are essentially comparing the dynamics of the fluid across the SWNT diameters at the same pressure, while in this study we are comparing the dynamics of the fluid mixtures across the SWNT diameters at the same density. This will be explained in greater detail later in the article. Molecular dynamics is performed in the same fashion as in section 2.1 with a Langevin thermostat to control the temperature.

Table 1: Densities of mixtures studied as a function of argon mole fraction, x_{Ar} in (6,6), (7,7), (8,8), (9,9), and (10,10) armchair carbon nanotubes at 298 K. The nanotube lengths are 49.19 nm.

	ρ_{mix} / g/cm^3	
x_{Ar}	Ar/Kr	Ar/Ne
0	1.260	0.213
0.1	1.183	0.240
0.3	1.028	0.295
0.5	0.874	0.350
0.7	0.719	0.405
0.9	0.564	0.460
1	0.487	0.487

2.3 Pure Component argon confined in a (25,0) SWNT bundle

The bundle nanotube consists of (25,0) SWNTs with interstitial channel diameters of 0.354 nm and nanotube diameters of 1.95 nm (the geometric diameter of the (25,0) SWNT). The formula to determine the interstitial diameter can be found in [33]. GCMC simulations were performed to measure the adsorption isotherm of argon at 120 K in the relative pressure range of P/P_o = 1x10^{-6} to 0.1, where P_o is the bulk vapor pressure of argon at 120 K. This was calculated as 10.33 bar from the LJ equation of state [34] using the Lennard-Jones parameters of argon in this study. The unit cell lengths of the GCMC simulations were 4.58 nm, 3.97 nm, 11.06 nm in the x, y, and z directions, respectively. In the subsequent MD simulations, the system was replicated a number of times in the z direction to obtain approximately 10,000 interstitial atoms. The number of replications was determined by the density. Periodic boundaries were used in 3-dimensions. These simulations were equilibrated for 1 ns in NVT using a Nosé-Hoover thermostat with a 1 fs timestep, and production runs of 10 ns with a 1 fs timestep were performed in the microcanonical ensemble (NVE). The trajectory from the NVE production run was used to measure the mean squared displacement. These MD simulations were performed using the LAMMPS (Large-scale Atomic/Molecular Massively Parallel Simulator) simulation package [35].

3. Results

3.1 Pure component argon in SWNTs

The adsorption isotherms of argon confined in three types of chiralities of SWNTs at 298 K were calculated from GCMC simulations and are shown in Fig. 1. The loading is normalized using the accessible volume from Eq. (3). We observe a general trend that the loading decreases with increasing tube diameter, as it is less confined. However, in the (7,7), (12,0) and (8,6) tubes, the loading is at a minimum compared to the other tubes.

In these tubes, the diameter has increased compared to the (6,6), (10,0) and (7,5) SWNTs, but there is not enough space for a second molecular layer of fluid to adsorb. Therefore, the ratio of the amount of fluid adsorbed with respect to the accessible volume has decreased. In the zigzag chirality, there are two minimum diameters, (11,0) and (12,0) as this chirality of SWNT has a smaller increase in diameter compared to the other chiralities studied (armchair or chiral).

Several example configurations are shown as simulation snapshots in Fig. 2 at 30MPa and 298 K. In the (6,6), (10,0) and (7,5) SWNTs (diameters of approximately 0.8 nm), only a single molecular layer of fluid is adsorbed and this layer is almost linear along the SWNT axis. As the diameter increases slightly in the (7,7), (12,0) and (8,6) SWNTs (diameters of approximately 0.94 nm, accessible diameter approximately $1.76\sigma_{Ar}$), the fluid no longer aligns linearly with respect to the axial direction of the tube. However, the accessible volume is not large enough for a second molecular layer of fluid to form. As the diameter is increased further in the (9,9), (15,0) and (10,8) SWNTs with geometric diameters of approximately 1.2 nm, two molecular layers of fluid have formed.

Because, the (7,7), (12,0) and (8,6) SWNTs have the largest diameters that exhibit the single molecular layer of fluid, we refer to these as the "transition" or "crossover" SWNTs. All SWNTs studied with diameters larger than these transition nanotubes exhibited at least two molecular layers of fluid. We also find that the adsorption energy profiles of argon in (6,6), (10,0) and (7,5) exhibit one energy minimum while the energy profiles in the (7,7), (12,0) and (8,6) SWNTs exhibit two energy minima. The adsorption energy profiles of argon in SWNTs larger than the transition SWNT diameter exhibit at least two energy minima.

A second analysis of the isotherm can be obtained by plotting the accessible loading as a function of the SWNT diameter. This is shown in Fig 3 (a). A minimum in the loading occurs at a diameter of approximately 0.94 nm. This is the diameter corresponding to the (7,7), (12,0) and (8,6) SWNTs (the transition SWNTs). In Fig 3(b) we show the same plot, but only at 30 MPa for clarity. We find that below approximately 2 MPa, this minimum in the loading disappears. Therefore, we have limited our MD study to pressures above 2 MPa. Mon and Percus found a minimum in the density for hard sphere fluids in perfect cylinders with hard walls. They obtained a mimimum in the density at a diameter of approximately $2.16\sigma_{HS}$. Our result is similar despite the fact that we are using a Lennard-Jones potential for the fluid-wall interaction. We found that the minimum is at $2.76\sigma_{Ar}$ based on the geometric diameter of the SWNT or $1.76\sigma_{Ar}$ when the accessible diameter is taken into account from Eq. (3). We can conclude that the ratio of the diameter of the fluid compared to the SWNT diameter is an important factor in determining whether the fluid adsorbs in a single molecular layer.

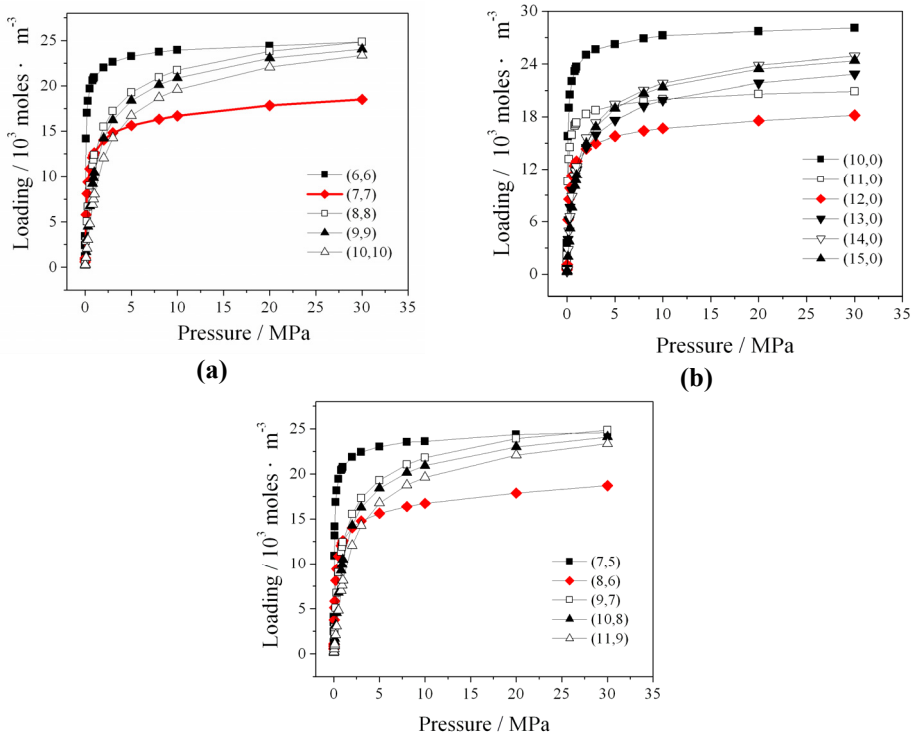

Fig. 1: Adsorption isotherms of argon confined in three types of chiralities in SWNTs at 298K. (a) armchair (b) zigzag (c) chiral. In each case the loading is reduced by the accessible volume (Eq. 3).

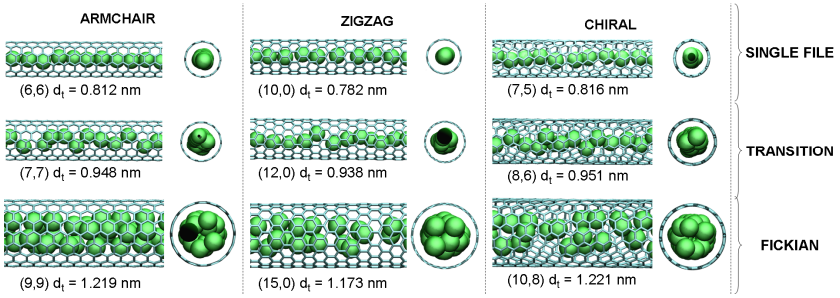

Fig. 2**:** Snapshots of GCMC simulations of argon confined in armchair, zigzag and chiral SWNTs at 298 K and 30 MPa.

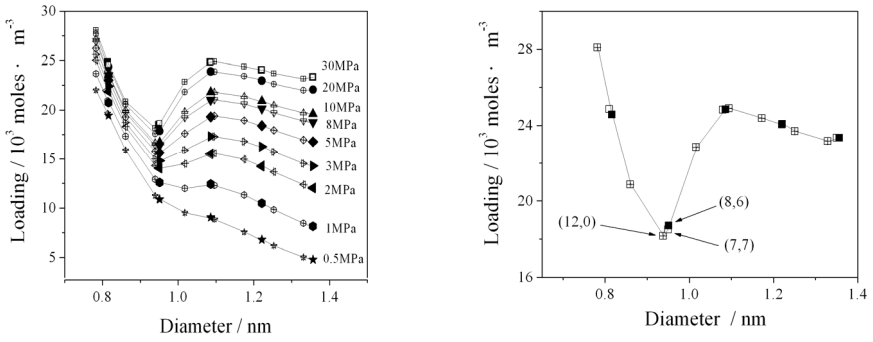

Fig. 3: (a) Loading of argon in three chiralities of SWNTs as a function of the diameter of the SWNTs at 298 K at pressures in the range of 0.5MPa to 30 MPa (armchair, open; zigzag, cross; chiral, closed) (b) Loading of argon in three types of SWNTs at 298 K as a function of the diameter at 30MPa (armchair, open; zigzag, cross; chiral, closed)

Diffusive motions in pores can occur by several fundamentally different mechanisms, including ballistic motion (Eq. 5), Fickian diffusion (Eq. 6), and single-file diffusion (Eq. 7).

$$\lim_{t\to 0}\left\langle \left[z(t)-z(0)\right]^2 \right\rangle = 2Et^2 \tag{5}$$

$$\lim_{t\to \infty}\left\langle \left[z(t)-z(0)\right]^2 \right\rangle = 2Dt \tag{6}$$

$$\lim_{t\to \infty}\left\langle \left[z(t)-z(0)\right]^2 \right\rangle = 2F\sqrt{t} \tag{7}$$

In Eqns. (5-7) z is the distance along the axial direction of the pore, the left hand side of these equations is the mean squared displacement of a molecule in time t, E is the ballistic mobility constant, F is the single-file mobility, and D is the familiar Fickian self-diffusion coefficient.

Clearly ballistic motion is much faster than Fickian diffusion, which is in turn much faster than single-file diffusion; the latter occurs when the pore is too narrow to allow molecules to pass each other. All three mechanisms are seen in our MD simulations. It is important to know which diffusion mechanism is occurring in the material. Many materials of current interest have a bi- or tri-modal pore distribution, so that more than one mechanism may be occurring in different regions of the material at the same time

Figure 4 shows the MSD of argon as a function of time in three chiralities of SWNTs at 30MPa. For all tubes, if the time is shorter then 1 ps, the MSD exhibits approximately ballistic motion. As time increases, in the larger tubes, which have diameters larger than 1.1 nm, the motion is Fickian, with the MSD proportional to time. For the small tubes with diameters of 0.814, 0.783 and 0.816 nm corresponding to the (6,6), (10,0) and (7,5) SWNTs, respectively, the MSDs are proportional to the square root of time, typical of SFD. The intermediate tubes with diameters of 0.949, 0.939 and 0.951

nm corresponding to the transition SWNTs of (7,7), (12,0) and (8,6), respectively, also have MSDs proportional to the square root of time. However, even though the MSD still is proportional to the square root of time in the transition SWNTs, which indicates SFD, the MSD is much larger compared to the (6,6), (10,0) or (7,5) SWNTs. The location of the MSDs of the transition SWNTs is intermediate between the Fickian and the smallest SFD SWNTs, and a crossover from single-file to Fickian diffusion occurs.

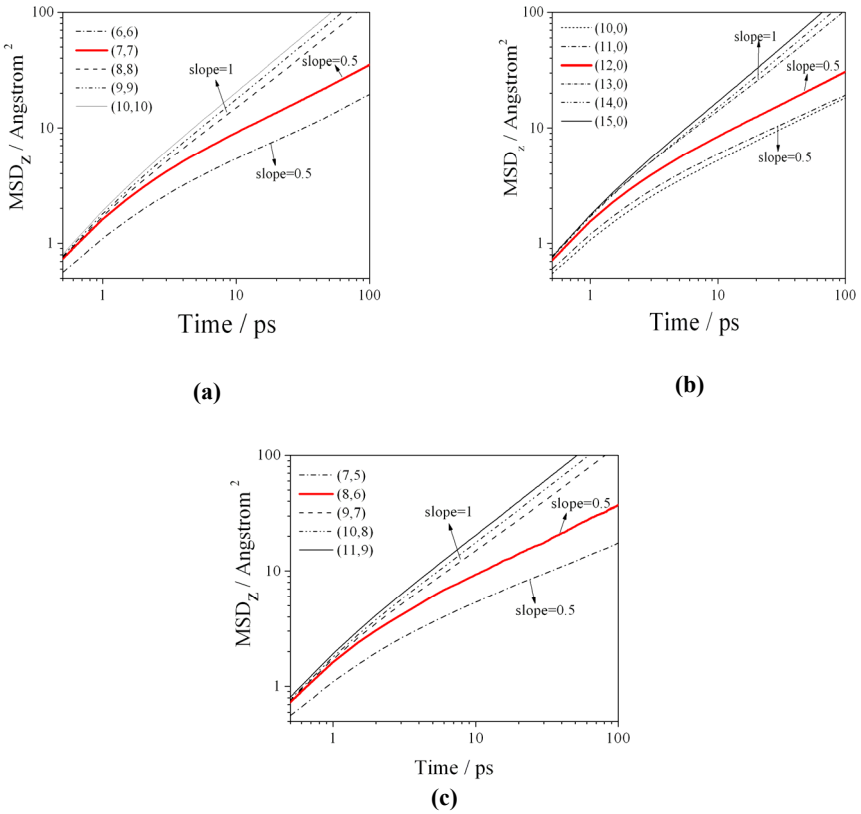

Fig. 4: Axial direction mean squared displacement (MSD) of argon confined in (a) armchair (b) zigzag (c) chiral SWNTs at 298 K and 30 MPa.

Note that in Fig 4., we have only shown the MSDs to 100 ps. As we have used a Langevin thermostat, which makes use of modifying the velocities randomly to correct the temperature, we have overcome some of the aspects associated with the finite size effects previously shown by Hahn and Karger [36] in single-file diffusion. Because of this, we were able to observe the $t^{1/2}$ dependence for the single-file fluids in the range of 10 to 100 ps for systems of the order of 100 atoms. However, the system size effects still exist and present themselves for times on the order of 1 ns for this system size.

In Fig. 5, three types of transport coefficients are shown as a function of pressure for different SWNTs. All coefficients decrease as presure increases and increase as tube size increases in the same chirality of SWNT. We compared the coefficients for the crossover and the single-file mobility for SFD which have the same units and magnitude. The diffusivities for the crossover point are larger than the SFD mobilities. The Fickian diffusivity is greater by four orders of magnitude than the single-file mobility, *F,* and crossover diffusivity. At these conditions, the effect of the chirality of the SWNTs is negligible. This is because the fluid-wall energy differences are small compared to *kT* for argon in these different chiralities at 298 K. For other fluids, such as water, the difference between diffusion coefficients in different chiralities of SWNTs at 298 K have been shown to be quite pronounced [37].

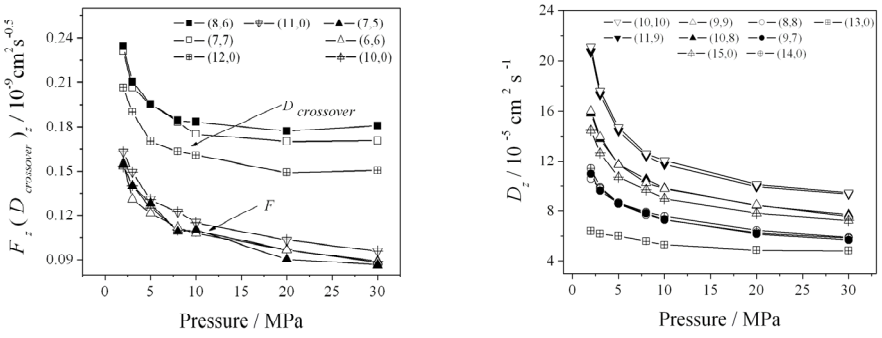

(a) **(b)**

Fig. 5: Transport coefficients of argon as a function of pressure in the various chiralities and diameters of SWNTs. (a) single-file mobility, F, and crossover diffusivity, $D_{\text{crossover}}$, (b) Fickian diffusivity.

3.2 Binary mixtures of argon/krypton and argon/neon

We have examined two binary Lennard-Jones mixtures, Ar/Kr and Ar/Ne. Examples of mean squared displacements for both mixtures are shown in Fig. 6. In the Ar/Kr mixture, both Ar and Kr have similar sizes ($\sigma_{\text{Ar}} = 0.342$ nm, $\sigma_{\text{Kr}} = 0.3607$). In the (6,6) and (7,7) nanotubes, both components exhibit single-file diffusion as shown in Fig. 6 (a) for Ar and Fig. 6 (b) for Kr. Neither component can pass itself or the other component. In the larger diameter SWNTs, the diffusion is Fickian, and both components can freely pass all other atoms. These results are similar to what we found for pure argon diffusing in SWNTs. The only difference of note is that the diffusion rate of both components in the (7,7) SWNT is the slowest. This is in contrast to the case of the pure component Ar diffusing in SWNTs. In the present case each mixture is compared at the same density in all of the SWNTs. In the case of pure component argon in 3.1, we found a minimum in the density in the (7,7) SWNT for argon, and thus the rate of diffusion was faster compared to the (6,6) SWNT. Since the density is the same in the (6,6) and (7,7) SWNTs, the (7,7) SWNT has a higher order of packing compared to the (6,6) SWNT

(because of the increased accessible volume), and thus the rate of the diffusion in the (7,7) SWNT is slower.

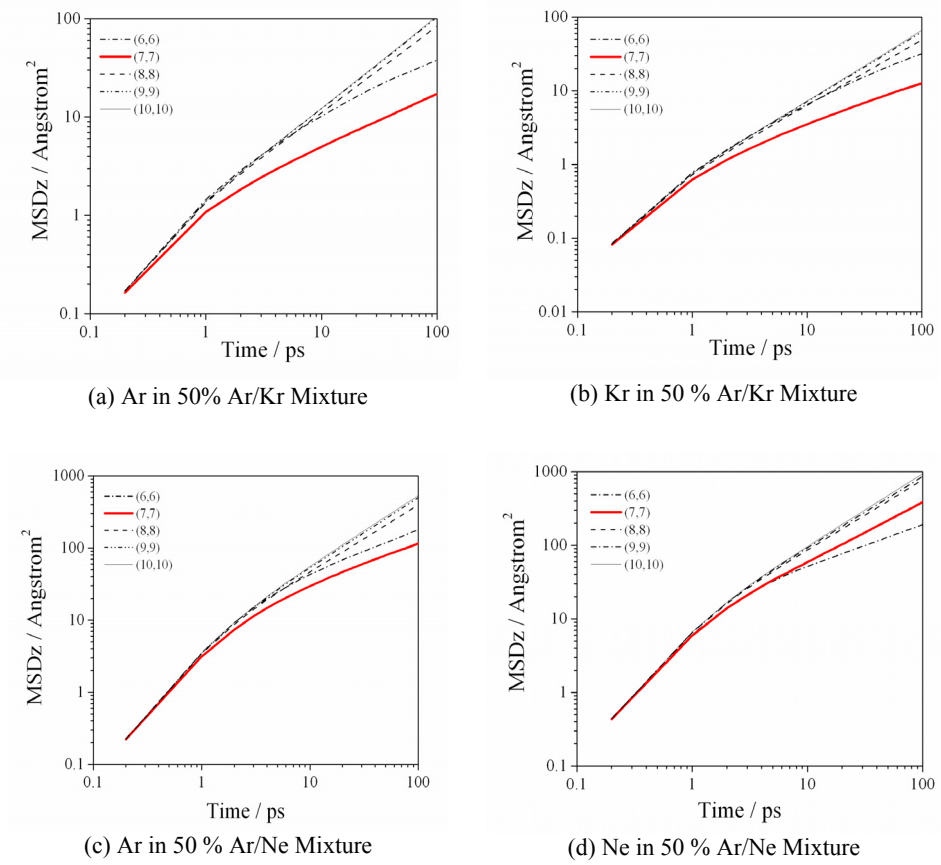

Fig. 6: Axial direction mean squared displacement (MSD) of (a) Ar in a 50 mole % Ar/Kr mixture; ρ_{mix} = 0.874 g/cm^3 (b) Kr in a 50 mole% Ar/Kr mixture; ρ_{mix} = 0.874 g/cm^3 (c) Ar in a 50 mole % Ar/Ne mixture; ρ_{mix} = 0.350 g/cm^3 and (d) Ne in a 50 mole % Ar/Ne mixture; ρ_{mix} = 0.350 g/cm^3 in armchair SWNTs at 298 K.

In Fig. 6 (c) and 6 (d) we show similar results for Ar in the Ar/Ne mixture. Argon has a mean squared displacement proportional to $t^{1/2}$ in the (6,6) and (7,7) SWNTs, indicative of SFD, and a mean squared displacement proportional to t^1 in the (8,8), (9,9), and (10,10) SWNTs, indicative of Fickian diffusion. Neon also has a mean squared displacement proportional to $t^{1/2}$ in the (6,6) SWNT, indicative of SFD and a mean squared displacement proportional to t^1, indicative of Fickian diffusion, in the (8,8), (9,9) and (10,10) SWNTs. However, in the case of the (7,7) SWNT, Neon has a mean squared

displacement proportional to t^1, indicative of Fickian diffusion. Therefore, in the case of the (7,7) SWNT, the Ar/Ne mixture provides an example of bimodal diffusion, where Ar is exhibiting SFD, while Ne is exhibiting Fickian diffusion. Bimodal diffusion has previously been observed for binary Lennard-Jones mixtures in molecular sieves [38], and recently for hard disks in structureless pores with hard walls [39].

Simulation snapshots are shown in Fig. 7. For the Ar/Kr mixture in Fig. 7(a) the snapshots for the (6,6) and (7,7) SWNTs indicate that both components are not able to pass themselves or the other component. In the (10,10) SWNT, both components are clearly able to pass and exhibit Fickian diffusion. In Fig. 7(b) both Ar and Ne in the Ar/Ne mixture are not able to pass in the (6,6) SWNT but in the (7,7) SWNT, Ar cannot pass itself or Ne, but Ne can pass itself and Ar, giving rise to the t^1 dependence in the mean squared displacement for Ne in Fig. 6(d).

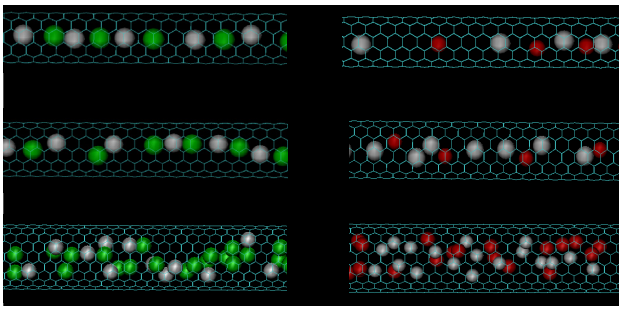

(a) Ar (white)/Kr (green) **(b)** Ar (white)/Ne (red)

Fig. 7: Simulation snapshots of (a) Ar/Kr mixtures and (b) Ar/Ne mixtures

The transport coefficients for each component are shown in Fig. 8 for both mixtures. In Fig. 8 (a) and Fig. 8 (c), the Fickian diffusion coefficients are reported, while in Fig. 8(b) and Fig. 8(d) the single-file mobilities are reported. For both components in the Ar/Kr mixture, the diffusion coefficients increase with increasing Ar concentration. This is the result of Kr having a larger mass than Ar. For both components in the Ar/Ne mixture, the diffusion coefficients decrease with increasing Argon concentration. This is the result of Ne having a smaller mass than Ar. Likewise, Ar diffuses faster than Kr, and Ne diffuses faster than Ar. At present it is not clear how to define a mutual diffusion coefficient for single-file diffusion [40], and therefore, mutual diffusion coefficients are not reported. Since the molecules are not substantially different in size or structure, it is possible that the mutual diffusion coefficients can be accurately approximated from the pure component self-diffusivities as $D_{AB} = x_A D_A + x_A D_B$, as has previously been reported for Ar/Kr mixtures in confinement [41].

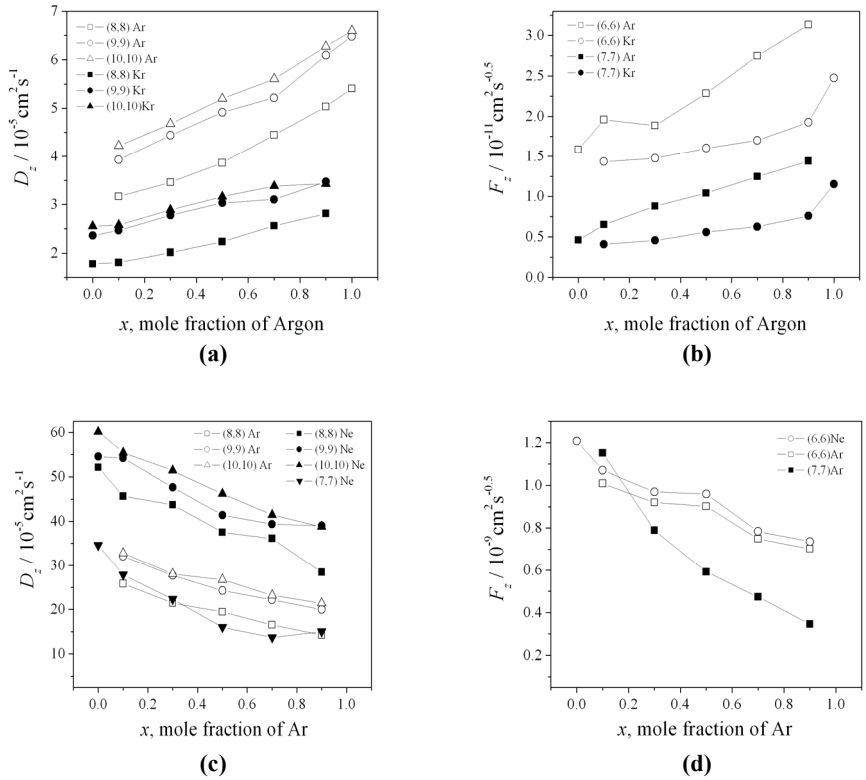

Fig. 8: (a) Fickian self-diffusion coefficients for Ar and Kr in Ar/Kr Mixtures at 298 K for (8,8) (9,9) and (10,10) SWNTs , (b) Single-file mobilities for Ar and Kr in Ar/Kr mixtures at 298 K for (6,6) and (7,7) SWNTs; (c) Fickian self-diffusion coefficients for Ar and Ne in Ar/Ne Mixtures at 298 K for (8,8) (9,9) and (10,10) and Ne in (7,7) SWNTs; (d) Single-file mobilities for Ar and Ne in Ar/Kr mixtures at 298 K for (6,6) SWNTs and Ar in (7,7) SWNTs

3.3 Pure component argon in a (25,0) SWNT bundle

There are two kinds of pore channels in SWNT bundles, the inner channels within the nanotubes and the interstices between nanotubes. In order to effectively characterize the properties of Ar adsorbed in different channels of SWNT bundles, a temperature of 120 K was chosen such that the filling of the different sites could be distinguished in the isotherm. Figure 9(a) shows the loading of Ar in SWNT bundles as a function of relative pressures at 120 K with Fig. 9(b) showing simulation snapshots at various relative pressures. The adsorption in the interstitial and inner channels are shown separately, as well as the total adsorption. At relative pressures lower than 0.00001, the particles adsorb only in the interstitial channels, since these are the strongest adsorption sites. As the pressure increases, the inner channels begin to fill with adsorbate, until at relative pressures close to 0.00005 the interstitial sites are almost completely filled. The inner

channels continue to fill with adsorbate as the pressure increases, and the bundle is almost completely filled at relative pressures close to 0.01.

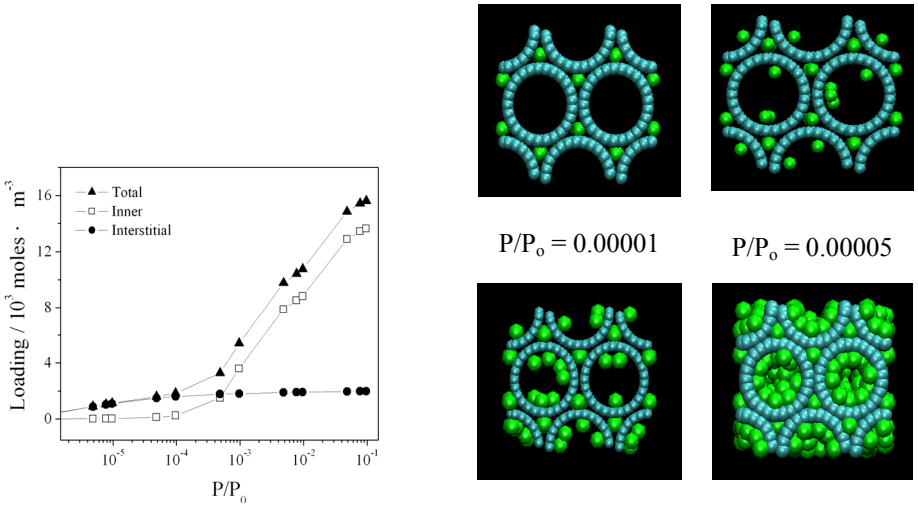

Fig. 9: Loading of argon in a bundle of SWNTs as a function of relative pressures at 120 K (a). Isotherm (b) Snapshots.

We have performed MD simulations of the systems shown in Fig. 9(b), and the mean squared displacements are shown in Fig. 10. In all cases we observe ballistic motion at sub-picosecond times changing to either Fickian or single-file motion at longer times, depending on the pore diameter. The pore size distribution is bimodal, with diffusion occurring within the pores and between pores in the interstices. The interstitial channel is 0.354 nm in diameter, only slightly larger than the molecular diameter of argon, so the particles in the interstitial sites cannot pass each other. Therefore, we observe all of the interstitial MSDs being proportional to the square root of time, indicating SFD. For fluids diffusing in the inner channels, the particles can pass each other and their MSDs are proportional to time, indicating Fickan diffusion.

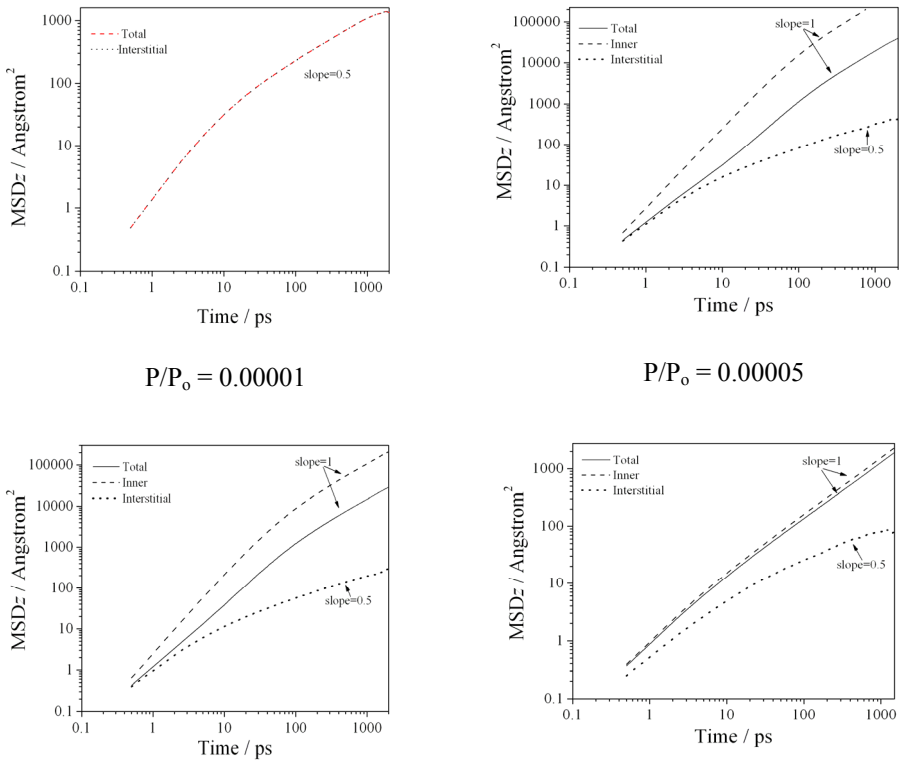

Fig. 10: Mean squared displacement (MSD) of Ar in the bundle of (25,0) SWNTs at 120 K and different relative pressures.

Although the total MSD of the system depends on both the rates of the diffusing interstitial and inner channel atoms, the total system MSDs for P/P_o greater than approximately 0.00001 are all proportional to time. This result may seem surprising as one might expect the slope to be between 1/2 and 1 on the log-log plot. However, due to the dramatic difference between the rates of Fickian and single-file diffusion, the total fluid MSD is dominated by the fluid in the nanotube (inner channel) at long times. Because the molecules are first adsorbed in interstitial channels and then the inner channels begin to fill as the pressure increases, the total fluid MSD becomes increasingly dominated by the inner channels as the pressure increases. No molecules are adsorbed in the inner channels at $P/P_o = 0.00001$, and the total MSD is equal to the interstitial MSD. As the pressure increases slightly, even though there are some molecules adsorbed in inner channels, the total MSD is dominated by interstitial fluid in the ballistic region at

short times for relative pressures of P/P_o = 0.00005 and 0.0001. At longer times, the total fluid MSD separates from the interstitial MSD, finally achieving Fickian behavior. However, as the pressure is further increased and more particles begin to fill the inner channels at P/P_o = 0.0001, the total fluid MSD becomes closer to the MSD of the inner channel atoms. Finally, as the bundle has almost completely been filled with fluid at P/P_o = 0.01, the fluid in the inner channel dominates the total fluid MSD even in the ballistic region. When the bundle is almost completely filled, the total fluid MSD approaches that of the inner channel. These explanations are confirmed in Fig. 11, showing the Fickian diffusion coefficients for the diffusing inner channel atoms and the total fluid as well as the single-file mobilities (insert of Fig. 11) of the interstitial atoms. The diffusion coefficients and single-file mobilities decrease with increasing pressure. The diffusion coefficient of the total fluid decreases until it approaches that of the inner channel at P/P_o = 0.01.

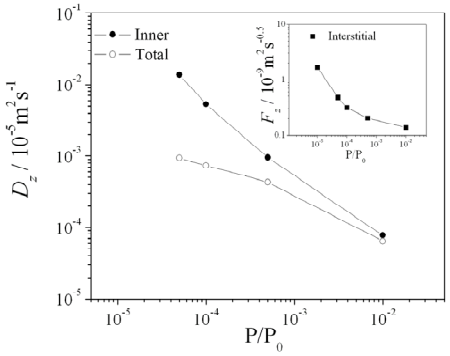

Fig. 11: Transport coefficients for Ar in the SWNT bundle at 120 K and different relative pressures. Single-file mobilities, F, for the interstitial atoms are shown in the insert.

4. Conclusion

Carbon nanotube structures provide a model to investigate the diffusion mechanism of self-diffusion known to occur in small pores. Ballistic motion always occurs for short times (sub-picosecond), and Fickian or single-file diffusion occurs at longer times depending on the pore size. We found that argon diffuses in single-file for SWNT diameters less than approximately 0.94 nm or approximately $1.76\sigma_{Ar}$ in accessible diameter, corresponding to (7,7), (12,0) and (8,6) SWNTs in our study. For SWNTs with diameters larger than these, we observe Fickian diffusion. Previous studies have reported slopes of the MSD on the log-log scale between 1/2 and 1 possible for chain molecules diffusing in SWNTs [42], but despite analyzing incrementally increasing pore diameters, we found that the slope does not deviate from 1/2 for single-file diffusion and 1 for Fickian diffusion for argon.

In mixtures of LJ fluids, we find that mixtures of similar size (Ar/Kr) provide single-file diffusion of both components in (6,6) and (7,7) SWNTs and Fickian diffusion of both

components in SWNTs of larger diameters. For binary mixtures of Ar/Ne, we found that the (6,6) SWNTs give rise to single-file diffusion of both components. However, because of the greater deviation of the molecular diameters of Ar and Ne, in the (7,7) SWNT Ar diffuses in single-file while Ne diffuses in 3-dimensions, passing itself and Ar. This is an example of bi-modal diffusion in a binary mixtures. For SWNTs larger than (7,7) both Ar and Ne diffuse in a Fickian fashion.

Carbon nanotube bundles provide an example of a pore structure with a bimodal pore distribution. In a (25,0) SWNT bundle, Ar can diffuse in single-file in interstitial sites and in a Fickian fashion in the inner nanotube channels. While the adsorption first occurs in the interstices at low pressures followed by pore filling in the inner channels at higher pressures, the total diffusion of fluid in the bundle is always dominated by Fickian diffusion in the inner channels at longer times. While the interstitial sites provide a slope of the MSD on the log-log scale the diffusion for the interstitial sites of 1/2 and for the inner channels of 1, the total bundle MSD always has a slope of 1 when fluid has adsorbed in the inner channels.

All of our SWNTs are rigid in this study. Our preliminary studies using flexible nanotubes show very little effect of flexibility on the diffusion mechanism or coefficients at the conditions considered here. (Keil and coworkers [43-47] have observed larger effects of nanotube flexibility for low pressure Knudsen diffusion).

4. Acknowledgements

We wish to thank Benoit Coasne, Erik Santiso, and Martin Schoen for helpful discussions. This work was supported by the U.S. National Science Foundation (grant number CTS-0626031) and the National Natural Science Foundation of China (No. 20876132 and 50576080). Computational time was provided at the San Diego Supercomputing Center by the U.S. National Science Foundation (grant. no. CHE080046N).

References

[1] T. Kaneko, Y.F. Li, S. Nishigaki, R. Hatakeyama, J. Am. Chem. Soc. 130 (2008) 2714-2715

[2] L.H. Guan, K. Suenaga, S. Iijima, Nano Lett. 8 (2008) 459-462.

[3] B.J. Hinds, N. Chopra, T. Rantell, R. Andrews, V. Gavalas, L.G. Bachas, Science 303 (2004) 62-65.

[4] J. Chaste, L. Lechner, P. Morfin, G. Feve, T. Kontos, J.M. Berroir, D.C. Glattli, H. Happy, P. Hakonen, B. Placais, Nano Lett. 8 (2008) 525-528.

[5] P. Kowalczyk, R. Holyst, Environ. Sci. Technol. 42 (2008) 2931-2936.

[6] V. Gupta, S. Nivarthi, A. McCormick, H.T. Davis, Chem. Phys. Lett. 247 (1995) 596-600.

[7] Q.-H. Wei, C. Bechinger, P. Leiderer, Science 287 (2000) 625-627.

[8] R. Allen, S. Melchionna, J.-P. Hansen, Phys. Rev. Lett. 89 (2002) 175502(1)- 175502 (4).

[9] G. Hummer, J.C. Rasaiah, J.P. Noworyta, Nature, London 414 (2001) 188-190.

[10] C. Wei, D. Srivastava, Phys. Rev. Lett. 91 (2003) 235901(1)- 235901(4).
[11] O.G. Jepps, S.K. Bhatia, D.J. Searles, Phys. Rev. Lett. 91 (2003) 126102(1)-126102(4).
[12] V.P. Sokhan, D. Nicholson, N. Quirke, J. Chem. Phys. 120 (2004) 3855-3863.
[13] K.F. Czaplewski, T.L. Reitz, Y.J. Kim, R.Q. Snurr, Microporous Mesoporous Mater. 56 (2002) 55-64.
[14] V. Kukla, J. Kornatowski, D. Demuth, I. Girnus, H. Pfeifer, L.V.C. Rees, S. Schunk, K.K. Unger, J. Kärger, Science 272 (1996) 702-704.
[15] K. Hahn, J. Kärger, V. Kukla, Phys. Rev. Lett. 76 (1996) 2762(1)-2762(4).
[16] H. Jobic, K. Hahn, J. Kärger, M. Bee, A. Tuel, M. Noack, I. Girnus, G. J. Kearley, J. Phys. Chem. B 101 (1997) 5834-5841.
[17] C. Lutz, M. Kollman, C. Bechinger, Phys. Rev. Lett. 93 (2004) 026001(1)-026001(4).
[18] K.K. Mon, J.K. Percus, J. Chem. Phys. 117 (2002) 2289-2292.
[19] K.K. Mon, J.K. Percus, J. Chem. Phys. 119 (2003) 3343-3346.
[20] K.K. Mon, J.K. Percus, J. Chem. Phys. 112 (2000) 3457-3458.
[21] (a) O.F. Sankey, P.A. Fedders, Phys. Rev. B, 15 (1977) 3586-3591. (b) P.A. Fedders, O.F. Sankey, Phys. Rev. B, 15 (1977) 3580-3585.
[22] J. Kärger, Phys. Rev. A, 45 (1992) 4173-4174.
[23] J.K. Percus, Phys. Rev. A 9 (1974) 557-559.
[24] D.G. Levitt, Phys. Rev. A 8 (1973) 3050-3054.
[25] K.K. Mon, J.K. Percus, J. Chem. Phys. 125 (2006) 244704(1)- 244704(5).
[26] K.K. Mon, J.K. Percus, J. Chem. Phys. 127 (2007) 094702(1)- 094702(3).
[27] A.I. Skoulidas, D.S. Sholl, J. Phys. Chem. B 106 (2002) 5058-5067.
[28] W.A. Steele, The Interaction of Gases With Solid Surfaces, Pergamon Press, Oxford, 1974.
[29] N. Hamada, S.I. Sawada, A. Oshiyama, Phys. Rev. Lett. 68 (1992) 1579(1)- 1579(4).
[30] J.C. Phillips, R. Braun, W. Wang, J. Gumbart, E. Tajkhorshid, E. Villa, C. Chipot, R.D. Skeel, L. Kale, K. Schulten, J. Comput. Chem. 26 (2005) 1781-1802.
[31] http://webbook.nist.gov/chemistry
[32] N. Chennamsetty, H. Bock, K.E. Gubbins, Mol. Phys., 103 (2005) 3185-3193.
[33] L. Ju, Y. Sidney, J. Chem. Phys. 119 (2003) 2376-2385.
[34] J.K. Johnson, J.A. Zollweg, K.E. Gubbins, Molec. Phys. 78 (1993) 591-618.
[35] S.J. Plimpton, J. Comput. Phys. 117 (1995) 1-19.
[36] K. Hahn , J. Kärger, J. Phys. Chem. 100 (1996) 316-326.
[37] Y.C. Liu, J.W. Shen, K.E. Gubbins, J.D. Moore, T. Wu, Q. Wang, Phys. Rev. B. **77** (2008) 125438(1)- 125438(7).
[38] D.S. Sholl, K.A. Fichthorn, J. Chem. Phys. 107 (1997) 4384 – 4389.
[39] C.D. Ball, N.D. MacWilliam, J.K. Percus, R.K. Bowles, J. Chem. Phys. 130 (2009) 054504(1)- 054504(6).
[40] C.R. Kamala, K.G. Ayappa, S. Yashonath, Phys. Rev. E., 65 (2002), 061202.
[41] L. Zhang, Y.C. Liu, Q. Wang, J. Chem. Phys., 123 (2005) 144701.
[42] Z. Mao, S.B. Sinnott, J. Phys. Chem B., 104 (2000) 4618-4624.

[43] S. Jakobtorweihen, M.G. Verbeek, C.P. Lowe, F.J. Keil, B. Smit, PRL, 95 (2005), 044501(1)- 044501(4).
[44] S. Jakobtorweihen, C.P. Lowe, F.J. Keil, B. Smit, J. Chem. Phys. 124 (2006) 154706(1)- 154706(13).
[45] S. Jakobtorweihen, C.P. Lowe, F.J. Keil, B. Smit, J. Chem. Phys. 127 (2007) 024904(1)- 024904(11).
[46] N.E.R. Zimmermann, S. Jakobtorweihen, E. Beerdsen, B. Smit, F.J. Keil, J. Phys. Chem. C. 111 (2007), 17370-17381.
[47] S. Jakobtorweihen, F.J. Keil, B. Smit, J. Phys. Chem. B, 110 (2006) 16332-16336.